SPLASHING OF WATER DROPLETS ON A TILTED FLOWING LIQUID FILM

He Zhao*, Romain Ecault°, Carlos Alberto Dorao*, Svend Tollak Munkejord°

*Department of Energy and Process Engineering, Norwegian University of Science and Technology (NTNU), Kolbjørn Hejes vei 1B, 7491 Trondheim, Norway
°SINTEF Energy Research, Sem Sælands vei 11, 7465 Trondheim, Norway

ABSTRACT
An experimental investigation of water droplets impinging with a liquid film of water flowing on a 20°-tilted aluminium board was carried out. The effects of impinging droplet size, velocity and liquid film parameters on splashing were both qualitatively and quantitatively studied and discussed. The evolution of a non-symmetric crown was characterized by investigating the normalized crown height and a non-symmetry factor versus the normalized time, and the breakup of secondary droplets was found influential to the crown evolution. An increase of film velocity and depth reduced the crown height, but it does not affect the non-symmetry factor until the crown started to collapse. Threshold of splashing was investigated, and it was found that the threshold can be well described by the model reported in Ref. [4].

INTRODUCTION

Droplet impacting on a surface was studied since the end of 19th century [1], and there has been a substantial progress in understanding the droplet impact phenomena in the last two decades [2] owing to the development in the technology of high speed camera. Distinguishing different flow regimes was one of the most important purposes due to its contribution to the control of different processes such as fuel injection, inkjet printing, phase separation etc. Such works were related with both high energy impingement corresponding to splashing and jetting and low energy impingement corresponding to bouncing on either a dry surface [3][10] or a liquid-covered surfaces [4][5][8][9]. Another highlighted purpose was to study the evolution process of the droplet impact for establishing models, and such work can also be found for droplets impinging on a dry surface [11] and a liquid-covered surface impact [6].

One aspect in common for most of the droplet impact studies was that the targets on which droplets impacted were immobile, but in some industrial processes this is less likely to be true. One example is annular flow, in which droplets are torn off from and deposit to a flowing liquid film dynamically such as shown in Figure 1. Annular flow models without considering the dynamics of the dispersed phase fail in describing the parameters such as pressure drop, film thickness and heat transfer. This is also the case for other processes where a flowing liquid film and droplets interact with each other. In order to make robust models, one shall understand further the interactions between droplets and a flowing liquid film.

Studies of droplets impacting with a flowing liquid film are, however, found to be inadequate. Initial attempts are made in Ref. [12][13][14], of all which the impact conditions are nearly

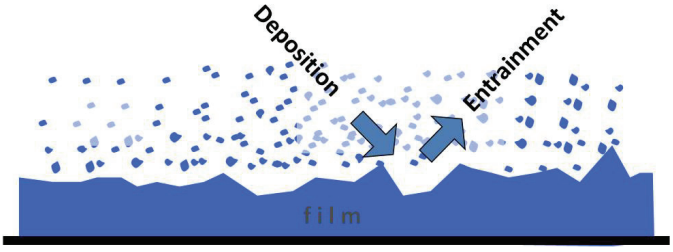

Figure 1 Sketch of annular-mist flow.

normal (tilted angle less than 10°, with a horizontal surface defined as 0°). Ref. [12][13] focused on studying the relationship between the size of the crater formed by the impact of the droplet and the dependence of the total volume of secondary drops on the thickness and velocity of the liquid layer, and the slope of the tray. Ref. [14] focused on the transitions of flow regimes, and the critical Weber numbers for characterizing the regime-transitions seem to be independent on both the film thickness and velocity reported in the article. It is thus desired to investigate the impact of droplets on a flowing liquid film with more tilted angles and velocities as to investigate the effects of non-symmetrical impact and liquid film parameters on splashing evolution and transition.

EXPERIMENTAL METHODS AND PARAMETERS

Experimental apparatus

Experimental apparatus and methods are to be described in this section. A sketch of the experimental apparatus is shown in

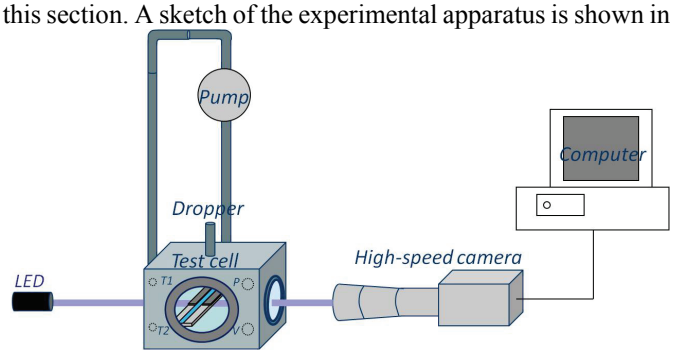

Figure 2 Sketch of experimental apparatus.

Figure 2. A collimated LED was served as a light source. A Phantom V9 digital camera operated at 1255 fps (in most of the acquisitions) with a resolution of 1440×1080 pixels was employed for capturing the droplet-film interactions. A 20°-tilted aluminum board was placed inside a test cell, and a shallow channel, in which a liquid film flowed, was made of one pair of aluminum foil bands. The channel width was 15.5 mm, and depth was decided by the thickness of the aluminum foil, which was about 0.1 mm. A liquid pump circulated water for generating a flowing liquid film. Droplet was generated from a dropper, a needle of gauge 33 (Hamilton). Droplet releasing height was varied in order to have different impinging velocities.

Measurement methods and parameters

Droplet diameter and velocity were measured from the captured videos. Diameter was evaluated by using the cross-sectional area of the droplet, and velocity was calculated by using the displacement and time interval. The relative uncertainties for both the diameter and velocity measurements were approximately 3%.

Four flow rates, 1.82×10^{-6}, 3.08×10^{-6}, 4.32×10^{-6}, 6.82×10^{-6} m^3/s were used. Liquid film thickness was evaluated by comparing the image difference with and without a liquid film. The relative uncertainty of the thickness was dependent on the flow rate, and the lowest and highest flow rates (1.82×10^{-6} and 6.82×10^{-6} m^3/s) corresponds to an uncertainty about 10%, while the other two flow rates (3.08×10^{-6}, 4.32×10^{-6} m^3/s) corresponds to an relative uncertainty about 5%.

Surface velocity of the liquid film was measured by tracking polybutylene beads (0.25-0.35 mm), which were set in the upstream of the flow. The relaxation time of the beads (τ_r) was less than 5 ms, which was about 10 times shorter than the time taken for the beads travelling from the released point to the camera focus, and thus, the beads can follow the flow well. The relative uncertainty of the surface velocity for the two lower flow rates (1.82×10^{-6}, 3.08×10^{-6} m^3/s) was about 5%, and was approximately 12% for the other two flow rates (4.32×10^{-6}, 6.82×10^{-6} m^3/s).

Table 1 shows the film parameters, in which the measured quantities are flow rate (Q), thickness (Δ), surface velocity (V_s), and the calculated quantities are mean velocity (V_m) and the film Reynolds number (Re_f) shown by Eq. (1) and Eq. (2).

$$V_m = \frac{Q}{\Delta \cdot W} \tag{1}$$

$$\mathrm{Re}_f = \frac{4\rho Q}{\mu W} \tag{2}$$

Table 1 Liquid film flow rate (Q, m^3/s) and corresponding liquid film thickness (Δ, mm), surface velocity (V_s, m/s), mean velocity (V_m, m/s) and Reynolds number (Re_f).

NO.	Q	Δ	V_s	V_m	Re_f
1	1.82×10^{-6}	0.55	0.37	0.21	528
2	3.08×10^{-6}	0.73	0.47	0.28	893
3	4.32×10^{-6}	0.89	0.55	0.32	1253
4	6.82×10^{-6}	1.20	0.62	0.38	1978

where Q, Δ and W are flow rate, thickness and channel width shown by, where $\rho = 1000$ kg/m^3 and $\mu = 0.89$ mPa·s are density and viscosity of water at 25°C.

EXPERIMENTAL OBSERVATIONS

In this section, we first show typical observations for the non-splashing regime, which is next to the regime of splashing. Secondly, splashing regime is shown, and the effects of droplet parameters, i.e. diameter and velocity, as well as the effects from the liquid film on splashing are described.

Non-splashing

For droplet-pool interactions, the non-splashing regimes can be jetting, coalescence, bouncing and partial coalescence. Jetting, which is adjacent to splashing and characterized by the central jet formation (sometimes breakup) [5][14], is of interest here. Figure 3 shows the typical non-splashing.

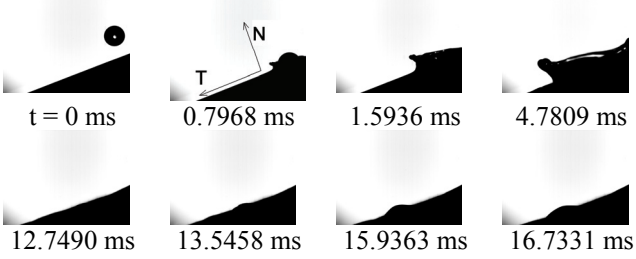

Figure 3 The non-splashing regime adjacent to splashing. Droplet parameters: diameter 2.0 mm, impinging velocity 2.8 m/s. Film parameters: angle 20°, thickness 0.55 mm, surface velocity 0.37 m/s (other parameters see Table 1).

Figure 3 shows that a non-symmetric wave is formed at t = 0.7968 ms. Due to the fact that the tangential (T) velocity of the droplet (≈ 1 m/s) is higher than the film velocity (0.37 m/s), the droplet has a relative motion towards downstream, along the tangential direction, of the liquid film, and thus a higher

wave (in the normal direction and relative to the undisturbed film surface thereinafter) can be expected and seen at the downstream side of the impact point. At t = 4.7809 ms, the leading edge of the wave develops to about the maximum height. A primary central jet is initially seen at t = 12.7490 ms, and it reaches its maximum height at approximately t = 15.9363 ms.

Different from the central jet formation with a normal impact, where the central jet appears at the impact point, the central jet formed here moves away from the impact point, and it appears at downstream of the impinging point. This owes to the oblique impact condition and the liquid film motion.

Another remarkable difference between the central jet formation here and that from droplet-pool interactions is that the primary jet does not disintegrate into secondary droplets. Ref. [16][17] reported no central jet formation for splashing on thin films (dimensionless film thickness $\Delta^* = \Delta / D$ less than 0.125, where D is diameter of droplet), and Ref. [17] proposed the reasons 1. Crown breaking led to energy loss. 2. No cavity collapse. With thicker films (Δ^* approx. 0.3~0.6) presented in this investigation, the primary jet is observed without breaking up. We suggest that ability of focusing the receding wave as to form and break up the central jet here is weaker than in the case of droplet-pool interaction due to two reasons: 1. Shallow film - unlike the impact on a pool, where an undisturbed crater is formed and collapses naturally, the crater formation is interrupted by an unyielding surface, and the wave expands radially, which reduces the mass focusing during receding. 2. Non-symmetric wave - the tilted surface and film movement form a non-symmetric wave, with which the ability of focusing the receding mass is weaker than with a more symmetric wave.

Splashing with different impinging velocities

In this part, the effect of the impinging velocity on splashing is to be examined with fixed film parameters and a fixed impinging droplet size. Figure 4 and Figure 5 show the impacts with the same droplet diameter (2.0 mm) and film parameters (angle 20°, thickness 0.55 mm, surface velocity 0.37 m/s, other parameters see Table 1) but with different impinging velocities.

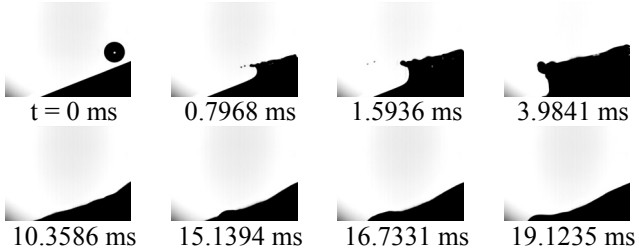

Figure 4 Splashing with impinging droplet diameter 2.0 mm, velocity 3.4 m/s.

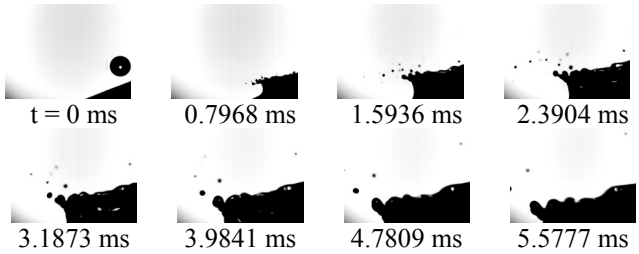

Figure 5 Splashing with impinging droplet diameter 2.0 mm velocity 3.9 m/s.

Comparing the first row of Figure 4 with Figure 5, one can readily see the differences that an increased velocity makes – more released secondary droplets from the crown breakup and also higher evoked crown height. It can also be seen that the released secondary droplets in Figure 5 have greater velocity components in the normal direction than the two released secondary droplets shown in Figure 4.

Figure 4 shows that the maximum crown height (of the leading edge thereinafter) is reached at around t = 3.9841 ms, and in Figure 5, the maximum crown height is reached at t = 4.7809~5.5777 ms, which is 1-2 frames delayed compared to the lower velocity case. This is because that all the secondary droplets in Figure 4 are formed at a time-point (t = 0.7968 ms, defined as single-stage breakup), which should be noted that this is not the exact moment due to the non-continuity of the picture-taking but shall be characterized by a certain frame in a video, while in Figure 5, secondary droplets are released at multiple time-points (t = 0.7968, 1.5936 and 3.1873 ms, defined as multi-stage breakup). The multi-stage breakup leads to the postponement of reaching the maximum crown height.

Figure 4 also shows that a primary central jet is initially seen at approximately t = 10.3586 ms and reaches its maximum height at about t = 19.1235ms, and this time is dramatically longer than the jetting case shown in Figure 3 (at t = 15.9363 ms). Therefore, time required for reaching the maximum jetting height is prolonged in the splashing case perhaps due to the breakup of secondary droplets.

Splashing with different impinging drop sizes

In this section, we shall examine the effects of varying droplet size on splashing with fixed film parameters the same as in the above section and a fixed impinging velocity at 3.9 m/s. Figure 5 will be referred as the splashing with a larger droplet diameter (2.0 mm), and Figure 6 shows a splashing with a lower droplet diameter (1.6 mm).

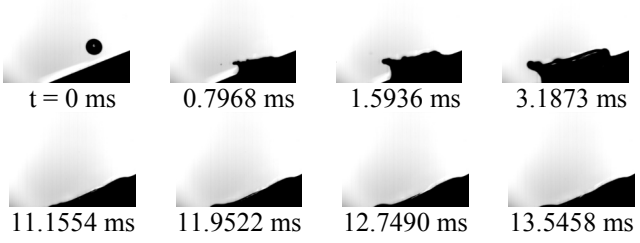

Figure 6 Splashing with impinging droplet diameter 1.6 mm and velocity 3.9 m/s.

It is obvious that a smaller droplet leads to the single-stage breakup of crown with less secondary droplets generation. The time for reaching the maximum crown height is at about t = 3.1873 ms, which is earlier than that in the splashing with multi-stage breakup in Figure 5.

Splashing with different film parameters

Effects of film parameters on splashing will be illustrated in this section, and Figure 5 will be employed to show the splashing with a liquid film flowing at a lower flow rate (thickness 0.55 and surface velocity 0.37 m/s). Figure 7 shows a splashing with the same impinging droplet diameter and velocity as those listed in Figure 5 but on a film with a higher flow rate (thickness 1.20 and surface velocity 0.62 m/s).

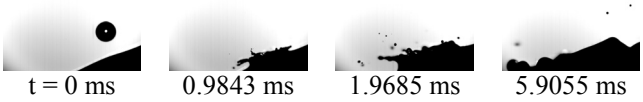

Figure 7 Splashing with film number 4: angle 20°, thickness 1.20 mm, surface velocity 0.62 m/s (other parameters see Table 1), droplet diameter and velocity are the same as those listed in Figure 5.

Figure 7 shows that the crown height is lower than that shown in Figure 5. Another noticeable difference is that the leading edge of the crown is more stretched towards the tangential direction as shown by the "filaments" at t = 0.9843 and 1.9685 ms.

The time required to reach the maximum crown height is at about t = 5.9055 ms, which is slightly delayed but not largely different from that in Figure 5, as both of the splashing cases experience multi-stage breakup.

EXPERIMENTAL ANALYSIS

Quantitative analysis of the impact evolutions

In this section, we shall analyze the crown height evolution of splashing. The normalized height of the leading edge of the crown (H_1^*) and the non-symmetry factor of the crown (S) as shown in Figure 8 are studied with the normalized time (t^*),

$$H_1^* = \frac{H_1}{D} \tag{3}$$

$$S = \frac{H_1}{H_2} \tag{4}$$

$$t^* = \frac{t \cdot V_n}{D} \tag{5}$$

where t and V_n are elapsed time and normal component of impinging velocity.

Figure 9 shows the crown development for splashing on a flowing liquid film (angle 20°, thickness 0.55 mm, surface velocity 0.37 m/s, other parameters see Table 1).

Figure 8 Sketch of splashing heights of leading edge (H_1) and trailing edge (H_2).

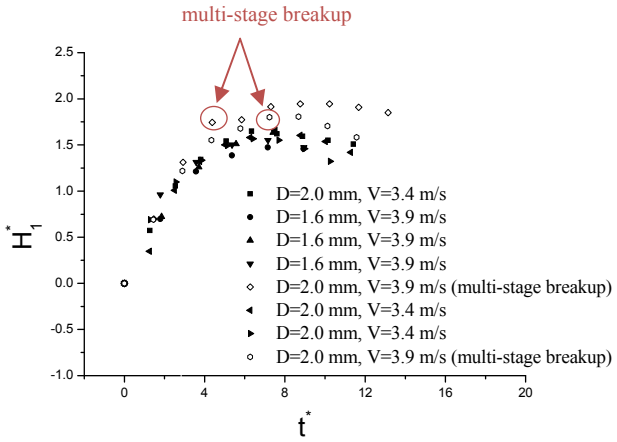

Figure 9 Crown evolution of splashing on a flowing liquid film (No. 1 in Table 1): effect of multi-stage breakup.

Figure 9 shows that crown evolutions with single-stage breakup follow nearly the same path, while the crown evolutions with multi-stage breakup deviate from that path at the moment that multi-stage breakup is formed. Due to the multi-stage breakup, a delayed maximum crown height is obtained. It can also be noted that the earlier multi-stage breakup tends to maintain the crown height at maximum, while the crown height drops faster in the case with the later multi-stage breakup during the collapse of crown.

Figure 10 illustrates the non-symmetry factor during the crown evolutions. As can be seen from the figure, this factor is maintained at about $S = 2$ while the crown height is growing (approx. for $t^* < 10$), and it increases fast as the crown starts to collapse. It reveals that the leading edge and trailing edge grow with a similar scale, while the trailing edge collapses with a larger scale.

Figure 11 shows the crown evolution for splashing on a flowing liquid film with a higher flow rate (angle 20°, thickness 1.20 mm, surface velocity 0.62 m/s, other parameters see Table 1), and the data shown in Figure 9 is plotted with grey colour. It is obvious that the increase of liquid film velocity and depth leads to a lower crown height formation. Multi-stage breakup is also observed, and it behaves in the similar way which makes the evolutionary curves of crown height deviate from the splashing with single-stage breakup.

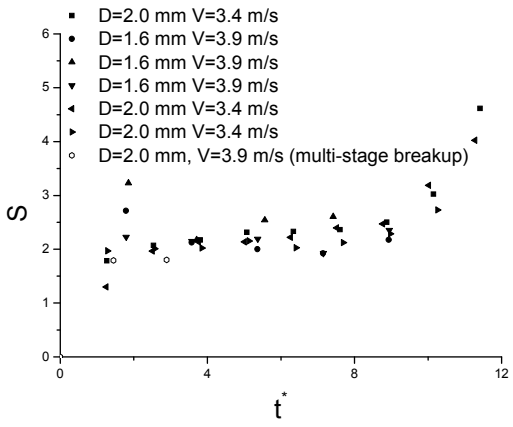

Figure 10 Non-symmetry factor of splashing on a flowing liquid film (No. 1 in Table 1).

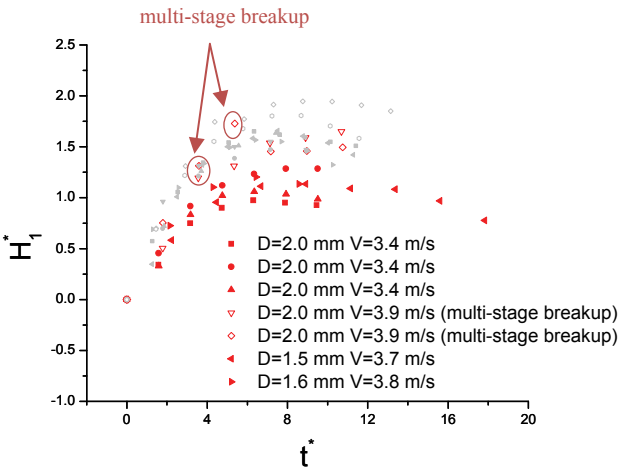

Figure 11 Crown height evolution of splashing on a flowing liquid film (No. 4 in Table 1), and grey symbols present the crown height evolution shown in Figure 9.

Figure 12 shows the non-symmetry factor for splashing on a flowing liquid film (angle 20°, thickness 1.20 mm, surface velocity 0.62 m/s, other parameters see Table 1), and the data shown in Figure 10 is plotted in grey colour. Little difference is seen between the non-symmetry factors of splashing on the two films during the crown height increase (approx. for $t^* < 10$), while the non-symmetry factor for the flowing film with a higher velocity and depth tends to continually stay at around $S = 2$ during the collapse of crown.

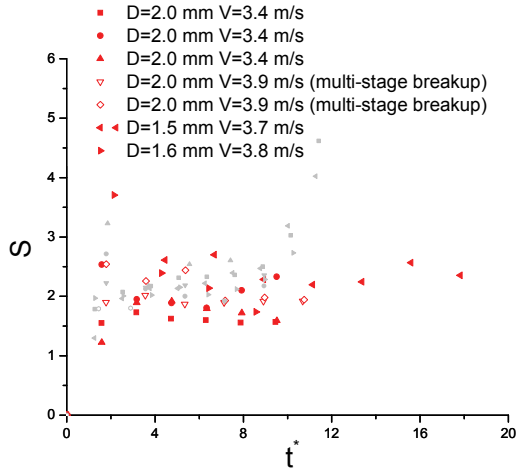

Figure 12 Non-symmetry factor of splashing on a flowing liquid film (No. 4 in Table 1), and grey symbols present the non-symmetry factor shown in Figure 10.

Splashing threshold

In the analysis of the threshold between splashing and jetting, only the data of splashing and jetting is of interest. The Ohnesorge number ($Oh = \mu/(\rho\sigma D)$, $\sigma = 72$ mN/m denotes the surface tension of water) range in the present investigation is $Oh \in [0.0023, 0.0036]$, and the dimensionless thickness is $\Delta^* \in [0.2, 0.9]$. Both of the parameters were comparable with the experiments of water in Ref. [4], which presented a model (6) for the critical Weber number (We_c), which distinguishes splashing and non-splashing.

$$We_c = \frac{2100 + 5880 \cdot \Delta^{*1.44}}{Oh^{-0.4}} \tag{6}$$

In the present investigation, the impact of droplets on to a 20°-tilted board was close to the normal impact condition regarding the comparison between the normal vector and the composite vector of the impinging Weber number. With a 20°-tilted board, the ratio between the normal vector ($We_{c,n}$) and the composite vector (We_c) of the critical Weber number is as follows.

$$\frac{We_{c,n}}{We_c} = \sin^2 70^\circ \approx 0.9 \tag{7}$$

Thus, if the motion of the liquid film is assumed to be not influential under the quasi-normal impact condition, the critical Weber number for a 20°-tilted board should be close to the critical Weber number predicted for a horizontal film-covered surface in Ref. [4].

Figure 13 shows the Weber number against the dimensionless thickness of the flowing liquid film. For comparison, the critical Weber number calculated using model (6) is plotted in the figure.

Figure 13 shows that the threshold of splashing and jetting for droplets impinging with a 20°-tilted board is, in general, well characterized by model (6). In fact, the threshold fits better the calculated value for $\Delta^* < 0.5$, and the experimental thresholds become to be overestimated by the model as dimensionless thickness increases. This agrees well with Ref. [4], in which the agreement between the model and experimental results is better for $\Delta^* < 0.3$ than for $\Delta^* > 0.5$, where the calculated threshold starts to be overestimated. Thus, the assumption is true that the effects of the liquid film motion on the threshold of splashing are not obviously seen for droplets impinging with a tilted flowing liquid film with a quasi-normal impact condition such as the 20° board inclination in the present study.

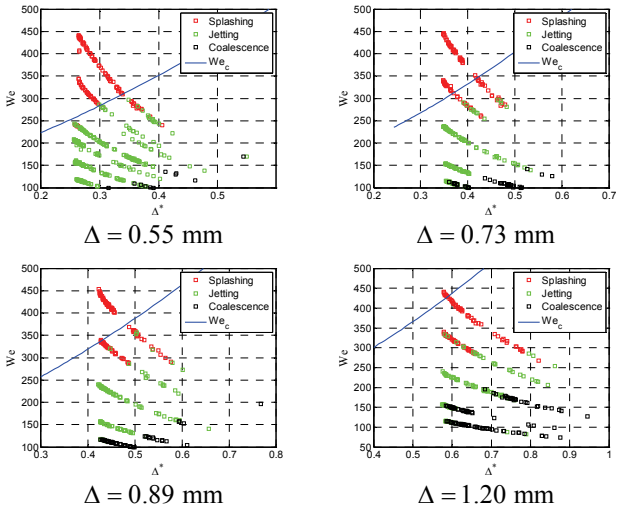

Figure 13 Weber number (We) versus dimensionless thickness (Δ^*) with comparison to the critical Weber number (We_c) calculated using model (6).

CONCLUDING REMARKS

An experimental investigation of water droplets impinging with a liquid film of water flowing on a 20°-tilted board was made with the focus on splashing evolution and threshold. The investigation showed that, for a given liquid film, an increase in either droplet diameter or velocity resulted in more secondary droplets from crown breakup. The crown evolutions with single-stage breakup followed a similar path, while those with multi-stage breakup deviated from this path with higher crown heights and delays in reaching the maximum crown heights. An increase in the film velocity and depth led to lower crown height.

The non-symmetric crown was characterized by a non-symmetry factor S, which was steady ($S \approx 2$) during the crown growing and increased during the crown collapse for a thin and slow-flowing film (NO. 1 in Table 1). With a thicker and faster-flowing film (NO. 4 in Table 1), this factor tended to maintain stable ($S \approx 2$) throughout both the crown growing and collapse.

The impact condition in this investigation was quasi-normal, and little difference in the splashing threshold from the normal impact was noticed as the critical Weber numbers can be well characterized by using the model (6) presented in Ref. [4]. However, the threshold model became less robust as the normalized film thickness is above 0.5.

ACKNOWLEDGMENT

This publication is based on results from the research project Enabling low emission LNG systems, performed under the Petromaks program. The authors acknowledge the project partners; Statoil and GDF SUEZ, and the Research Council of Norway (193062/S60) for support.

NOMENCLATURE

Symbol	Quantity	SI Unit
Δ	Film thickness	m
Δ^*	Dimensionless film thickness	
μ	Viscosity of water	Pa·s
ρ	Density of water	kg/m^3
σ	Surface tension of water	N/m
τ_r	Relaxation time	s
D	Droplet diameter	m
H_1	Crown height, leading edge	m
H_1^*	Dimensionless crown height, leading edge	
H_2	Crown height, trailing edge	m
Oh	Ohnesorge number	
Q	Flow rate	m^3/s
Re_f	Film Reynolds number	
S	Non-symmetry factor	
t	Elapsed time	s
t^*	Dimensionless time	
V	Impinging velocity	m/s
V_f	Film velocity	m/s
V_m	Mean velocity of film	m/s
V_n	Normal component of impinging velocity	m/s
V_s	Surface velocity of film	m/s
W	Width of channel	m
We	Weber number	
We_c	Critical Weber number	
$We_{c,n}$	Normal component of critical Weber number	

REFERENCES

[1] A.M. Worthington, On the Forms Assumed by Drops of Liquids Falling Vertically on a Horizontal Plate, *Proc. R. Soc. Lond.*, vol. 25, pp. 261-272, 1876.

[2] A.L. Yarin, Drop Impact Dynamics: Splashing, Spreading, Receding, Bouncing…, *Annu. Rev. Fluid Mech.*, vol. 38, pp. 159-192, 2006.

[3] C. Mundo, M. Sommerfeld and C. Tropea, Droplet-Wall Collisions: Experimental Studies of the Deformation and Breakup Process, *Int. J. Multiphase Flow*, vol. 21 (2), 151-173, 1995.

[4] G.E. Cossali, A. Coghe and M. Marengo, The Impact of a Single Drop on a Wetted Solid Surface, *Exp. Fluids*, vol. 22, pp. 463-472, 1997.

[5] H. Zhao, A. Brunsvold and S.T. Munkejord, Investigation of Droplets Impinging on a Deep Pool: Transition from Coalescence to Jetting, *Exp. Fluids*, vol. 50 (3), pp. 621-635, 2011.

[6] A. Bisighini, G.E. Cossali, C.Tropea and I.V. Roisman, Crater Evolution after the Impact of a Drop onto a Semi-infinite Liquid Target, *Phys. Rev. E*, vol. 82 (3), pp. 036319, 2010.

[7] F. Blanchette and T.P. Bigioni, Partial Coalescence of Drops at Liquid, *Nat. Phys.*, vol. 2, pp. 254-257, 2006.

[8] K.L. Pan and C.K. Law, Dynamics of Droplet-Film Collision, *J. Fluid Mech.*, vol. 587, pp. 1-22, 2007.

[9] H. Zhao, A. Brunsvold and S.T. Munkejord, Transition between Coalescence and Bouncing of Droplets on a Deep Liquid Pool, *Int. J. Multiphase Flow*, 2011, Accepted.

[10] D. Bartolo, F. Bouamrirene, É. Verneuil, A. Buguin, P. Silberzan and S. Moulinet, Bouncing or Sticky Droplets: Impalement Transitions on Superhydrophobic Micropatterned Surfaces, *Europhy. Lett.*, vol. 74 (2), pp. 299, 2006.

[11] Š. Šikalo and E.N. Ganića, Phenomena of Droplet–Surface Interactions, *Exp. Therm. Fluid Sci.*, vol. 31 (2), pp. 97-110, 2006.

[12] V.G. Sister, O.A. Eliseeva, and A.K. Lednev, Study of the Features of Impact Reaction of a Droplet with a Liquid Surface, *Chem. Pet. Eng.*, vol. 45 (5-6), pp. 271-274, 2009.

[13] V.G. Sister, O.A. Eliseeva, and A.K. Lednev, Formation of Secondary Drops upon Collision of a Drop with a Liquid Surface, *Chem. Pet. Eng.*, vol. 45 (7-8), pp. 473-477, 2009.

[14] S.K. Alghoul, C.N. Eastwick and D.B. Hann, Normal Droplet Impact on Horizontal Moving Films: an Investigation of Impact Behaviour and Regimes, *Exp. Fluids*, vol. 50 (5), pp. 1305-1316, 2011.

[15] S.K. Alghoul, C.N. Eastwick and D.B. Hann, Normal Droplet Impact on Horizontal Moving Films: an

Investigation of Impact Behaviour and Regimes, *Exp. Fluids*, vol. 50 (5), pp. 1305-1316, 2011.
[16] D.A. Weiss and A.L. Yarin, Single Drop Impact onto Liquid Films: Neck Distortion, Jetting, Tiny Bubble Entrainment, and Crown Formation, *J. Fluid Mech.*, vol. 385, pp. 229-254, 1999.
[17] A.B. Wang and C.C. Chen, Splashing Impact of a Single Drop onto Very Thin Liquid Films, *Phys. Fluids*, vol. 12 (9), pp. 2155-2158, 2000.